Computational methods for wave-structure interaction

Numerical analysis of a RBF-based method

Nielsen, Morten Eggert

Publication date:
2020

Document Version
Publisher's PDF, also known as Version of record

COMPUTATIONAL METHODS FOR WAVE-STRUCTURE INTERACTION

NUMERICAL ANALYSIS OF A RBF-BASED METHOD

BY
MORTEN EGGERT NIELSEN

DISSERTATION SUBMITTED 2020

AALBORG UNIVERSITY
DENMARK

Computational methods for wave-structure interaction

Numerical analysis of a RBF-based method

PhD Dissertation

Morten Eggert Nielsen

Dissertation submitted August 31, 2020

Dissertation submitted: August 31, 2020

PhD supervisor: Professor Lars Damkilde
Aalborg University

PhD committee: Associate Professor Peter Frigaard (chairman)
Aalborg University

Professor Harry B. Bingham
DTU Mechanical Engineering

Professor Peter Troch
Ghent University

PhD Series: Faculty of Engineering and Science, Aalborg University

Department: Department of Energy Technology

ISSN (online): 2446-1636
ISBN (online): 978-87-7210-802-5

Published by:
Aalborg University Press
Kroghstræde 3
DK – 9220 Aalborg Ø
Phone: +45 99407140
aauf@forlag.aau.dk
forlag.aau.dk

Printed in Denmark by Rosendahls, 2020

Preface

The present PhD thesis, "Computational methods for wave-structure interaction: Numerical analysis of a RBF-based method", has been completed during my PhD study from September 2016 to August 2020 at the Department of Civil Engineering, Aalborg University, Denmark. The thesis is presented as a collection of papers that have been written therewhile.

Acknowledgements

First and foremost, I would like to thank my supervisor, Professor Lars Damkilde, for his guidance and patience throughout my PhD study. He always supported and motivated the exploration of new ideas, which made the study a very rewarding process.

I would also like to express my gratitude to Professor Bengt Fornberg for hosting me as a visiting scholar at the Department of Applied Mathematics, University of Colorado, Boulder, USA. It was a true pleasure to experience his innovative mindset and inspiring persona. Furthermore, I would like to thank Dr. Daniel Appelö who contributed very positively to my stay at CU Boulder, and Dr. Natasha Flyer for showing her hospitality and generosity from the very first day I arrived at the airport.

Finally, I want to thank my nearest and dearest for their continuous moral support and helpfulness during my study. I cannot even begin to quantify the importance and my appreciation of this.

Morten E. Nielsen
Aalborg University, Esbjerg, August 31, 2020

Abstract

This project aims to advance the state of the art within computational methods for wave-structure interaction problems. This is attempted by developing a new method for non-linear potential flows, which is based on radial basis function-generated finite differences (RBF-FD). The new RBF-based method is investigated due to its high-order accuracy and mesh-free nature, which makes it possible to discretize the governing partial differential equations on unstructured node sets that conform with the time-dependent free surface and other moving boundaries.

Unstructured node sets and nearest neighbor stencil selections will in general result in asymmetric stencils. These asymmetric stencils give rise to temporal instabilities as the eigenvalues of the discrete gradient operator will not be purely imaginary. This numerical issue can be remedied by adding dissipative terms to the free surface conditions. In this thesis, the dissipative terms are based on hyperviscosity, which is a high-order Laplace operator that seeks to stabilize the system without deteriorating the accuracy.

Hyperviscosity works by shifting the spurious eigenvalues, i.e. eigenvalues related to highly oscillatory eigenvectors, towards the left half of the complex plane, while leaving the physical eigenvalues intact. The amount by which the eigenvalues are shifted depends on the scaling of the hyperviscosity operator. This scaling parameter is in general problem dependent, but it is shown that a heuristic scaling law can be derived based on the Nyquist frequency in combination with an approximate ℓ_1 normalization of the hyperviscosity operator.

Near boundaries the heuristic scaling law may give rise to instabilities. However, these instabilities are related to irregularities in the scaling parameters rather than the asymmetric stencils. Thus, the temporal stability can be improved by smoothing out the irregularities, e.g. by applying a moving median filter, when boundaries are intersecting the free surface. This smoothing operation leaves the eigenspectrum globally intact, while shifting the eigenvalues with large real parts even further towards the left half of the complex plane.

The proposed stabilization technique in combination with the developed node generation and update strategy, which enables node refinements towards the free surface and other moving boundaries, results in a stable computational method suitable for non-linear wave-structure interaction problems. Preliminary two-dimensional test cases show promising results, which illustrate the

potential of the proposed method and further investigations are encouraged.

Resumé

Dette projekt sigter efter at bidrage til state of the art inden for beregningsmetoder til bølge-struktur interaktions problemer. Dette er forsøgt opnået ved at udvikle en ny metode til ikke-lineær potential strømninger, som er baseret på radial basis function-generated finite differences (RBF-FD). Den nye RBF-baserede metode er undersøgt grundet dens højere-ordens nøjagtighed og net-fri natur, hvilket gør det muligt at diskretisere de styrende partielle differentialligninger på ustrukturerede knude sæt, som former sig efter den tidsafhængige fri overflade samt andre bevægelige rande.

Ustrukturerede knude sæt og nærmeste nabosøgninger vil generelt føre til asymmetriske diskretiseringer. Disse asymmetriske diskretiseringer giver anledning til ustabile løsninger eftersom egenværdierne af den diskrete gradient operator ikke udelukkende er imaginære. Dette numeriske problem kan undgås ved at tilføje absorberende led til randbetingelserne for den fri overflade. I denne afhandling er de absorberende led baseret på hyperviskositet, som er en højereordens Laplace operator, som søger at stabilisere systemet uden at forværre nøjagtigheden.

Hyperviskositet fungerer ved at forskyde ikke-fysiske egenværdier, dvs. egenværdier tilhørende stærkt svingende egenvektorer, mod den venstre halvdel af det komplekse plan, hvorimod fysiske egenværdier efterlades intakte. I hvilket omfang egenværdierne forskydes afhænger af skaleringen af hyperviskositets operatoren. Denne skalering afhænger generelt af problemet, men det er vist, at en heuristisk skaleringslov kan udledes ved at kombinere Nyquist frekvensen med en approksimeret ℓ_1 normalisering af hyperviskositets operatoren.

I nærheden af rande kan den heuristiske skaleringslov give anledning til ustabiliteter. Disse ustabiliteter er dog relateret til irregulariteter i skaleringsparametrene, frem for den asymmetriske diskretisering. Stabiliteten kan derfor forbedres ved at udjævne disse irregulariteter, fx ved at benytte et median filter, såfremt rande gennemskære den fri overflade. Denne udjævningsoperation efterlader egenspektrummet globalt intakt, medens egenværdierne med store realdele forskydes yderligere mod den venstre halvdel af det komplekse plan.

Den foreslåede stabiliseringsmetode kombineret med den udviklede knude generings- og opdaterings strategi, som muliggør forfinelse af knuder i nærheden af den fri overflade og andre bevægelige rande, udmønter sig i en stabil beregn-

ingsmetode egnet til ikke-lineære bølge-struktur interaktions problemer. Indledende to-dimensionale test problemer viser lovende resultater, som illustrerer potentialet af den foreslåede metode og opfordrer til yderligere undersøgelser.

Thesis details

Thesis title:
Computational methods for wave-structure interaction: Numerical analysis of a RBF-based method

PhD student:
Morten Eggert Nielsen

PhD supervisor:
Professor Lars Damkilde

The main body of this thesis is composed of the following papers:

[A] **M. E. Nielsen**, L. Damkilde, Stabilized radial basis function-generated finite differences for wave-structure interaction in bounded domains, Manuscript submitted to Applied Ocean Research (2020).

[B] **M. E. Nielsen**, B. Fornberg, L. Damkilde, Stabilized radial basis function-generated finite differences for fully non-linear water waves, Manuscript submitted to Journal of Computational Physics (2020).

[C] **M. E. Nielsen**, B. Fornberg, L. Damkilde, A high-order and mesh-free computational model for non-linear water waves, VIII International Conference on Computational Methods in Marine Engineering, 2019.

[D] **M. E. Nielsen**, L. Damkilde, Meshless Methods for Potential Flow Past a Circular Cylinder, Nordic Seminar on Computational Mechanics 30, 2019.

In addition to the main papers, the following project-related publications have been made:

- **M. E. Nielsen**, M. D. Ulriksen, L. Damkilde, SOFIA - A simulation tool for bottom founded and floating offshore structures. Procedia Engineering 199 (2019) 1308-1313.
- **M. E. Nielsen**, M. D. Ulriksen, L. Damkilde, Simulation of Floaters in Action - Theory (vol. 1). Department of Civil Engineering, Aalborg University, 2016.
- M. D. Ulriksen, D. Bernal, **M. E. Nielsen**, L. Damkilde, Damage localization in offshore structures using shaped inputs, Procedia Engineering 199 (2017) 2282-2287.

Contents

Part I

Extended summary

Chapter 1

Introduction

Parts of this chapter are based on the work in [A,B,C,D].

The goal of this project is to advance the state of the art within computational methods for wave-structure interaction problems by developing a new non-linear potential flow solver, which is high-order accurate, geometrically flexible and robust. The work presented in this thesis constitutes the proof-of-concept of the new solver, which is based on stabilized radial basis function-generated finite differences.

1.1 Background and motivation

Floating offshore wind turbines, wave energy converters, floating bridges, ships and subsea installations. Indisputably, the interaction between marine structures and ocean waves is of interest to many industries and has been a research topic for many years. Computational methods are used extensively for analyzing wave-structure interaction problems, including floating structures for which considerable non-linear effects may arise. Before reviewing state-of-the-art computational methods for the analysis of marine structures, some causes of non-linear behavior related to floating structures are briefly introduced.

From a structural perspective, the mooring system may introduce significant non-linear behavior. The main objective of mooring systems is station keeping or stabilization. Floating structures that include mooring systems are e.g. floating offshore wind turbines, wave energy converters, floating bridges and tunnels. In figure 1.1, a floating structure is illustrated along with its mooring system. As the floating structure may experience displacements due to incident waves, it will eventually pull the buoy, which will pull the mooring lines connected to it. Thus, the motion of the floating structures will increase or decrease the tension forces in the mooring lines, but also modify the referential configuration considerably if large motions are experienced. These motions will thereby influence the structural stiffness and change the dynamic behavior of the system.

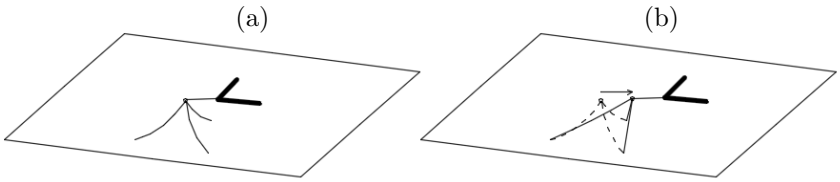

Fig. 1.1: A sketch of a moored floating structure in (a) initial configuration and (b) displaced configuration, which introduces geometrically non-linear behavior of the mooring lines [1].

Hydrodynamic loads do not only depend on the sea state conditions, but also the instantaneous spatial position of the floating structure within the given sea state. If the floating structure displaces considerably from its initial configuration, e.g. as illustrated in figure 1.2, the resulting hydrodynamic loads have to be computed by integrating the pressure field over the instantaneous wetted body surface. Thus, if large amplitude motion is experienced by the floating structure, the linear assumptions become invalid and non-linear motion have to be taken into account.

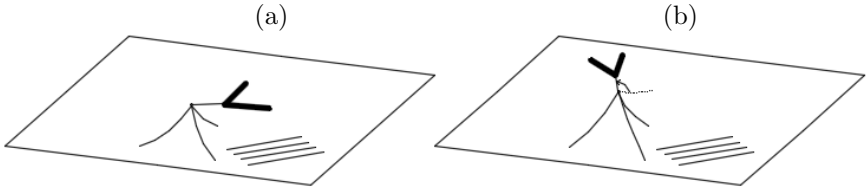

Fig. 1.2: A sketch of a moored floating structure exposed to incident waves that modify the floater orientation from (a) initial configuration to (b) displaced configuration [1].

The incident waves will influence the floating structures and the floating structure will influence the incident waves. However, the incident waves will only be notably affected if the size of the floating structure is comparable to the incident wave length. If this is the case, the floating structure will diffract the incident waves, but also radiate waves due to its motion, which can be effectively described in a linear setting. However, as the incident wave steepness and the floating structure motion increase, the linear assumptions break down.

In relation to viscosity, the main contribution to drag forces is flow separation, which may introduce significant non-linear forces. However, for large structures the drag forces may often be neglected because the fluid flow attaches to the body surface and the forces due to flow separation can be neglected.

1.2 Literature review

Many computational methods have been used to establish wave-structure interaction models [2]. A classification of different model fidelities are illustrated in figure 1.3.

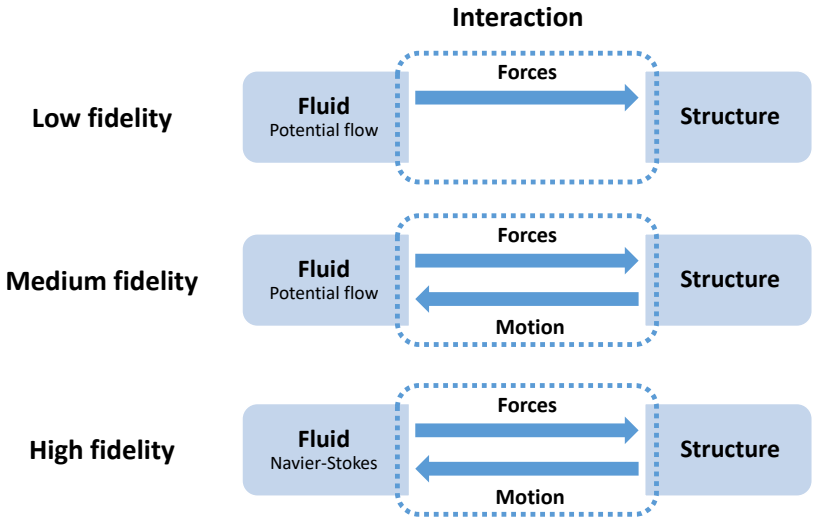

Fig. 1.3: Classification of model fidelities for wave-structure interaction problems.

Although high fidelity models include more features of the physical problem, it also comes at a higher computational cost as discussed in [2]. The higher cost is not always profitable if the most important features of the physical system can be sufficiently represented by a model with lower fidelity. In the following, the full range of computational methods are reviewed, although the non-linear potential flow models are the primary focus of this thesis [3]. An overview of non-linear hydrodynamic models for wave energy converters is given in [4].

1.2.1 Low fidelity models

Marine structures that are constructed by space frames are popular because of the load-bearing capacity to weight ratio. The slender tubular members are very small in comparison with the incident waves and therefore the structural members are assumed to be transparent to the incident waves. Thus, the hydrodynamic loads can be modeled by a semi-empirical relation, such as e.g. the Morison equation [5], which gives the approximated hydrodynamic forces based on particle kinematics computed with an applicable wave theory [5–8]. This approach is often implemented numerically, which makes it possible to allow for large amplitude motion of the structure and to include non-linear

contributions to the equation of motion [1,9,10]. This approach is also suitable for modeling the hydrodynamic loads on mooring lines [11, 12].

1.2.2 Medium fidelity models

Linear potential flow - frequency domain

Large floating structures can not be considered non-transparent to the incident waves. As the incident waves in operational conditions can be considered small in relation to the large floaters, the free surface elevation may be linearized about the mean water level, which leads to a single linearized free surface condition. This eases the solution of the flow field as the principle of superposition may be used in combination with potential flow theory. Hereby, the total flow field can written as the sum of an incident, diffraction and radiation velocity potential. The diffraction potential corresponds to the presence of a fixed body in incident waves, while the radiation potential corresponds to fluid motion due to body oscillations in still water [5–7]. In practice, the boundary element method (BEM) is typically used to solve for the relevant coefficients (added mass, radiation damping, hydrostatic stiffness, excitation forces) needed for describing the floater equation of motion in frequency domain [13, 14]. However, if important non-linear effects need to be included, it is necessary to solve the equation of motion in time domain.

Linear potential flow - time domain

The linear frequency domain approach is suitable for analysis of most operational conditions. However, linearization of external forces does not always provide suitable approximations, e.g. if non-linear mooring effects or non-linear viscous forces are expected. Especially for floating structures that consist of both large and small structural surface piercing elements, it is beneficial to combine the linear diffraction and radiation contributions with non-linear viscous contributions. To combine these terms, the equation of motion is solved in time domain, which is sometimes referred to as *Cummins' equation* due to the work in [15]. Similar to the frequency domain approach, the relevant coefficients can be computed by means of BEM codes [13, 14], but now also impulse response functions have to be computed. The resulting equations of motion have to be solved with a time integration scheme in a method-of-lines sense.

Fully non-linear potential flow

In linear hydrodynamics, the floating structures are assumed to experience small amplitude oscillations around their initial position, which means that the hydrodynamic forces are evaluated with respect to the initial configuration. Therefore, if the incident waves become steep or the floating structures experience substantial motion, the linear hydrodynamic models may become inaccurate. The model fidelity can be increased further by considering the fully

non-linear potential flow problem, which means that the non-linear free surface conditions are not linearized and the time-varying fluid domain has to be modeled.

The BEM is a popular choice in linear hydrodynamics, but it has also been a popular choice for non-linear wave propagation and wave-structure interaction problems [16–22]. As only the boundaries are discretixed, the BEM offers the geometric flexibility suitable for handling the moving boundaries of floating structures. This requires the Eulerian description of the free surface conditions to be exchanged with a semi- or fully Lagrangian frame of reference, which results in a Mixed Eulerian-Lagrangian (MEL) formulation. For this purpose, the BEMs fit well.

Finite differences on structured grids was originally presented in [23], where a time-invariant computational domain was used, at the cost of a Laplace equation with time-dependent coefficients. This model was later extended in [24,25] to include variable order finite differences with the possibility of grid stretching, e.g. for node clustering towards the free surface. Moving boundaries are not straight-forward to handle with traditional finite differences on time-invariant structured grids, and therefore a model based on the combination of finite differences and a weighted least squares (WLS) immersed boundary method was initially investigated in [26]. Further developments were presented in [27,28], where a time-invariant computational domain was used, but instabilities were noted near the intersection between the free surface and body boundaries. Thus, in [29] the model was extended by including a semi-Lagrangian formulation of the intersection point between the free surface and body boundaries. Although the robustness may have been improved, it is currently being investigated whether it is beneficial to leave out the time-invariant domain [30], which was also noted in the conclusions of the work in [28].

Another method that utilizes an immersed boundary method is the harmonic polynomial cell (HPC) method. The immersed boundary method is used to include arbitrary body boundaries in combination with overlapping grids [31–33].

Finite elements were used in [34–39] for wave propagation as well as wave-structure interaction. The models consist of the coupling between rigid body motion and a quasi arbitrary-Lagrangian-Eulerian finite element method (QALE-FEM) for the non-linear potential flow. The mesh is generated only once and then moved such that it conforms to the evolving boundaries, i.e. the free surface and moving boundaries. In this way, remeshing of the whole domain is circumvented by less costly local mesh movements at each time step.

Spectral elements have also been used to discretize the fluid domain [40–42]. In [40], temporal stability issues related to asymmetric meshes were investigated. It was proposed to add a dissipative term to the vertical kinematic free surface condition, which was scaled proportional to the mesh skewness. It was shown to be applicable to both linear and non-linear cases, where the Lagrangian free surface formulation was used. Instead of remeshing, the mesh was updated at each time step by solving two Laplace equations.

In [42], it was proposed to use a hybrid mesh as a remedy for instabilities related to the asymmetric mesh. The hybrid mesh consists of a layer of quadrilateral elements just below the free surface, while unstructured triangles are used in the remaining part of the domain. The free surface conditions are based on a Lagrangian formulation, which means that the mesh points have to be updated at each time step. This is done in a similar manner as in [36], where only mesh points close to moving boundaries are moved.

Although mesh-free methods provide the geometric flexibility needed for wave-structure interaction problems, not many potential flow solvers have been based on these methods. Radial basis function-generated finite differences (RBF-FD) [43–45], which is a mesh-free finite difference-like scheme, has only been used in few cases. One example is the numerical wave tank presented in [46], which utilizes the geometric flexibility of RBF-FD by solving the governing equations on a structured node set that moves proportional to the free surface elevation. Another example is the model presented in [47], which uses a time-invariant domain with RBF-FD discretization in the horizontal dimensions and a pseudo-spectral method in the vertical direction.

1.2.3 High fidelity models

Navier-Stokes/Euler equations

In order to include viscous effects, the Navier-Stokes equations or modified versions of these, e.g. Reynolds averaged Navier-Stokes (RANS) equations, have been used. These high fidelity models are often based on the finite volume method and require either an interface capturing or interface tracking method to resolve the free surface. An example of an interface capturing technique is the volume of fluid (VOF) method [48], which is suitable for representing multiphase flows. The air-water interface is captured by solving an additional transport equation that defines whether the individual cells contain air, water or a combination. An example of a model that tracks the free surface is the one presented in [49]. The model is based on WLS, while the Euler equations are formulated in an arbitrary-Lagrangian-Eulerian (ALE) frame of reference. The ALE-WLS model was developed for wave-structure interaction problems and wave-breaking events. Other models that are suitable for breaking free surfaces, and wave-structure interaction problems, are the ones based on smoothed particle hydrodynamics (SPH) [50, 51].

Hybrid formulations

Fully coupled fluid-structure interaction analysis based on Navier-Stokes equations is computationally expensive as noted in [52]. Thus, different domain decomposition strategies are being investigated in order to decrease the simulation time. The idea is to decompose the fluid domain into a far-field fluid domain and a near-field fluid domain. In the far-field the model with lowest

fidelity is used, while the model with the highest fidelity is used in the near-field. In [53], it was shown that significant computational speed-ups could be achieved by conducting a two-way coupling of far-field non-linear potential flow solver [25] and a SPH near-field solver [50]. A linear potential flow model was coupled with a submerged RANS domain in [54], which was used to improve the modeling of gap resonances, which may occur in moonpools or when floating structures are positioned in close proximity. Also, the QALE-FEM potential flow solver has been coupled with both a two-phase Navier-Stokes solver [55] and a SPH solver [56].

1.3 Hypothesis and objectives

From the literature review, it is found that the high fidelity models are still so computational costly that the non-linear potential flow solvers are of interest for many non-linear wave-structure interaction problems. Although the fully non-linear potential flow problem has been studied for many years, the development of efficient, accurate and robust computational methods is still an active research topic [2]. Lastly, it was also noticed that only a few studies investigated the use of RBF-FD in the context of fully non-linear potential flow problems, despite its high-order accuracy and geometric flexibility. Based on these findings, the following hypothesis is posed:

RBF-FD will provide a suitable framework for non-linear wave-structure interaction problems, due to its geometric flexibility and high-order nature, if sufficient temporal stability can be achieved on unstructured node sets.

The main objective of the thesis is to conduct a numerical analysis to assess whether RBF-FD is applicable to wave-structure interaction problems. The following objectives are defined for the hypothesis to be answered:

- Develop and implement a model for fully non-linear potential flow problems in 2D, which can handle moving boundaries.
- Investigate the numerical properties of the developed model.
- Investigate if hyperviscosity can be used to improve the temporal stability and how it affects the accuracy of the model.
- Investigate if a heuristic scaling law can be derived for the hyperviscosity operator.
- Validate the model using relevant test cases.

1.4 Outline

First, the mathematical formulation used for modeling the wave-structure interaction is introduced in chapter 2. The developed RBF-based method is introduced in chapter 3, which seeks to solve the problem posed in chapter 2. In chapter 4, the scientific contributions are described with reference to the publications made during the project. Finally, chapter 5 states the concluding remarks and presents suggestions for future research.

Chapter 2

Mathematical formulation

Parts of this chapter are based on the work in [A,B,C,D].

For irrotational flow of an incompressible and inviscid fluid, the potential flow theory is applicable. The governing Laplace equation can be obtained from the continuity equation such

$$\nabla^2 \phi = 0, \quad \boldsymbol{x} \in \Omega(t), \tag{2.1}$$

where $\nabla \in \mathbb{R}^d$ is the gradient operator, $\phi = \phi(\boldsymbol{x}, t) \in \mathbb{R}$ is the velocity potential and $\boldsymbol{x} \in \mathbb{R}^d$ is the position vector in a d-dimensional physical domain $\Omega = \Omega(t)$, as illustrated in figure 2.1.

2.1 Free surface conditions

Let $\Gamma_\eta = \Gamma_\eta(t)$ denote the free surface, then the kinematic and dynamic free surface boundary conditions can be expressed as

$$\frac{D\boldsymbol{r}}{Dt} = \boldsymbol{u}_p, \quad \boldsymbol{x} \in \Gamma_\eta(t), \tag{2.2}$$

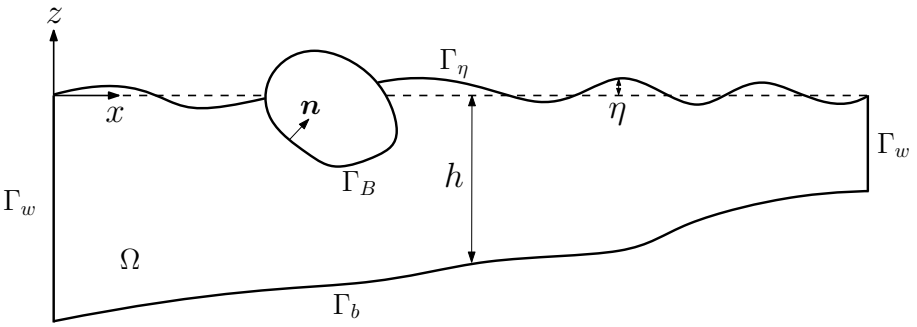

Fig. 2.1: Physical domain Ω with boundary definitions in $d = 2$.

$$\frac{D\phi}{Dt} = -g\eta - \frac{1}{2}\nabla\phi \cdot \nabla\phi + \boldsymbol{u}_p \cdot \nabla\phi, \quad \boldsymbol{x} \in \Gamma_\eta(t), \tag{2.3}$$

where g is the gravitational acceleration, $\boldsymbol{r} = (\boldsymbol{x}_h, \eta) \in \mathbb{R}^d$ is the free surface particle position vector, $\boldsymbol{x}_h = \boldsymbol{x}_h(t) \in \mathbb{R}^{d-1}$ is the horizontal position vector, $\eta = \eta(\boldsymbol{x}_h, t) \in \mathbb{R}$ is the free surface elevation and $\boldsymbol{u}_p \in \mathbb{R}^d$ is the free surface particle velocity vector given by

$$\boldsymbol{u}_p = \frac{\nabla\phi \cdot \boldsymbol{n}_\eta}{\boldsymbol{t}_w \cdot \boldsymbol{n}_\eta}\boldsymbol{t}_w, \tag{2.4}$$

with $\boldsymbol{n}_\eta \in \mathbb{R}^d$ being the unit vector normal to the free surface and $\boldsymbol{t}_w \in \mathbb{R}^d$ a unit vector that dictates the direction of the particle motion. This formulation is used due to the possibility of influencing the motion of free surface particles, which is beneficial if surface-piercing, and possibly moving, boundaries are present. As described in [16], the Eulerian formulation of the particle velocity is recovered by setting $\boldsymbol{t}_w = \boldsymbol{k}$ where $\boldsymbol{k}$ is a unit vector pointing in the positive vertical direction, while the Lagrangian particle velocity formulation is recovered by setting $\boldsymbol{t}_w = \nabla\phi / \left\|\nabla\phi\right\|_2$. The ability to blend a semi-Lagrangian and fully Lagrangian formulation is also interesting in respect to coupling with other methods, e.g. far-field solvers, where the free surface variables are often kept at fixed horizontal positions.

2.2 Fixed and moving boundaries

At the seabed, Γ_b, and other fixed boundaries, $\Gamma_w = \Gamma_w(t)$, the free-slip condition is enforced by

$$\boldsymbol{n} \cdot \nabla\phi = \frac{\partial\phi}{\partial n} = 0, \quad \boldsymbol{x} \in \left\{\Gamma_b \cup \Gamma_w(t)\right\}, \tag{2.5}$$

where $\boldsymbol{n} \in \mathbb{R}^d$ is a unit normal vector pointing out of the fluid domain. At moving boundaries, $\Gamma_B = \Gamma_B(t)$, the free-slip condition is enforced by

$$\frac{\partial\phi}{\partial n} = \boldsymbol{n} \cdot \boldsymbol{u}_B, \quad \boldsymbol{x} \in \Gamma_B(t), \tag{2.6}$$

with $\boldsymbol{u}_B = \boldsymbol{U} + \boldsymbol{\Omega} \times \boldsymbol{r}_B$ being the boundary velocity vector, assuming rigid body motion, $\boldsymbol{U} \in \mathbb{R}^d$ is the translational body velocity vector, $\boldsymbol{\Omega} \in \mathbb{R}^d$ is the angular body velocity vector and $\boldsymbol{r}_B \in \mathbb{R}^d$ is the position vector from the body's center of mass to the body surface. At intersection points, the boundary velocity is included in the particle velocity formulation in (2.4), such that

$$\boldsymbol{u}_p = \frac{(\nabla\phi - \boldsymbol{u}_B) \cdot \boldsymbol{n}_\eta}{\boldsymbol{t}_w \cdot \boldsymbol{n}_\eta}\boldsymbol{t}_w + \boldsymbol{u}_B, \tag{2.7}$$

where $\boldsymbol{t}_w$ defines the tangential direction of the boundary, which confines the particle motion to this direction.

2.3 Wave generation, absorption and ramping

Different techniques have been proposed for wave generation and absorption. In this work, the waves are generated and absorbed by an embedded penalty forcing technique [57], which was derived from a relaxation method in [58]. Thus, forcing terms are added to the free surface conditions, which for the dynamic free surface condition results in

$$\frac{D\phi}{Dt} = \mathcal{N}_\phi + \frac{1-\beta}{\Delta t}\left(\phi_a - \phi\right), \quad \boldsymbol{x} \in \Gamma_\eta(t), \tag{2.8}$$

where $\phi_a = \phi_a(\boldsymbol{x}, t)$ is the target value for the velocity potential, Δt is the time step size, $\mathcal{N}_\phi$ represents the right-hand side (RHS) of the dynamic free surface condition in (2.3) and $\beta = \beta(\boldsymbol{x})$ is a relaxation function [59] expressed as

$$\beta(\boldsymbol{x}) = \begin{cases} 1 - \frac{e^{d_g^{3.5}} - 1}{e-1}, & \boldsymbol{x} \in \Gamma_g = \{r_g < R_g\} \\ 1 - \frac{e^{d_d^{3.5}} - 1}{e-1}, & \boldsymbol{x} \in \Gamma_d = \{r_d < R_d\} \\ 1, & \text{otherwise,} \end{cases} \tag{2.9}$$

where R_g is the radius of the wave generation zone Γ_g, R_d is the radius of the wave absorption zone Γ_d, r_d is the horizontal distance to the origin of the wave absorption zone, r_g is the horizontal distance to the origin of the wave generation zone, $d_g = 1 - r_g/R_g$ is the normalized distance to the wave generation zone and $d_d = 1 - r_d/R_d$ is the normalized distance to the wave absorption zone. If simulations are initialized from still water level, the target values of the free surface variables are ramped according to the ramp function

$$\alpha(t) = \begin{cases} \frac{1}{2}\left(1 - \cos\left(\pi \frac{t}{t_r}\right)\right), & t < t_r \\ 1, & \text{otherwise,} \end{cases} \tag{2.10}$$

with the ramping period t_r. The target values of the free surface variables are multiplied by the ramp function such that they smoothly develop into the target sea state.

2.4 Pressure computation

The forces and moments on submerged structures can be computed by integrating the pressure over the wetted body surface,

$$\boldsymbol{f} = \int_{\Gamma_B(t)} p\boldsymbol{n}\, ds, \tag{2.11}$$

$$\boldsymbol{m} = \int_{\Gamma_B(t)} p(\boldsymbol{r} \times \boldsymbol{n})\, ds. \tag{2.12}$$

The unsteady Bernoulli's equation is used to compute the pressure,

$$p = -\rho \left(\phi_t + \frac{1}{2} \nabla\phi \cdot \nabla\phi + gz \right), \tag{2.13}$$

where $\phi_t = \phi_t(\boldsymbol{x}, t) \in \mathbb{R}$ is the partial time derivative of the velocity potential, which can be found in various ways. Here, it is computed by solving an additional Laplace equation, which can be derived from the acceleration potential [19, 20]. The acceleration potential is derived from Euler equations by expressing the fluid acceleration $\boldsymbol{a} \in \mathbb{R}^d$ as

$$\boldsymbol{a} = \frac{D\boldsymbol{u}}{Dt} = \frac{\partial \boldsymbol{u}}{\partial t} + (\boldsymbol{u} \cdot \nabla)\boldsymbol{u} = -\frac{\nabla p}{\rho} + g\nabla z, \tag{2.14}$$

which can be rewritten by expressing the velocity as $\boldsymbol{u} = \nabla\phi$, while using the vector identity

$$\frac{1}{2}\nabla(\boldsymbol{u} \cdot \boldsymbol{u}) = (\boldsymbol{u} \cdot \nabla)\boldsymbol{u} + \boldsymbol{u} \times (\nabla \times \boldsymbol{u}), \tag{2.15}$$

where $\nabla \times \boldsymbol{u} = 0$ due to the irrotationality assumption, such that

$$\boldsymbol{a} = \nabla\Phi = \nabla \left(\frac{\partial \phi}{\partial t} + \frac{1}{2}(\nabla\phi)^2 \right), \tag{2.16}$$

where $\Phi = \Phi(\boldsymbol{x}, t) \in \mathbb{R}$ is the acceleration potential. However, the velocity potential is already known, so only the partial time derivative of the velocity potential has to be computed. This can be computed by solving the additional Laplace problem

$$\nabla^2 \phi_t = 0, \quad \boldsymbol{x} \in \Omega(t). \tag{2.17}$$

On the free surface, the partial time derivative has to satisfy

$$\phi_t = -g\eta - \frac{1}{2}(\nabla\phi)^2, \quad \boldsymbol{x} \in \Gamma_\eta(t), \tag{2.18}$$

and at boundaries that experience pure translational motion,

$$\frac{\partial \phi_t}{\partial n} = \dot{\boldsymbol{U}} \cdot \boldsymbol{n} - k_n(\nabla\phi - \boldsymbol{U})^2 - \frac{\partial}{\partial n} \left(\frac{1}{2}(\nabla\phi)^2 \right), \quad \boldsymbol{x} \in \Gamma_B(t), \tag{2.19}$$

where $\dot{\boldsymbol{U}} \in \mathbb{R}^d$ is the translational body acceleration vector and k_n is the normal curvature of the body surface, which is $k_n = -1/R$ for a circular cylinder of radius R. For fixed boundaries the boundary condition is given as

$$\frac{\partial \phi_t}{\partial n} = -\frac{\partial}{\partial n} \left(\frac{1}{2}(\nabla\phi)^2 \right), \quad \boldsymbol{x} \in \{\Gamma_b \cup \Gamma_w(t)\}. \tag{2.20}$$

After having computed ϕ_t, the resulting forces and moments can be calculated according to (2.11) and (2.12), where the unsteady Bernoulli's equation has

been used to formulate the pressure. If the body motion is forced, the RHS of (2.19) is known after the velocity potential has been computed. However, if the pressure and the body motion are both unknown, it may be necessary to deal with added mass instabilities, which are caused by a too weak coupling between the body motion and the pressure. Only forced vertical motion is considered in this work, so added mass instabilities are not encountered.

Chapter 3

Stabilized radial basis function-generated finite differences

Parts of this chapter are based on the work in [A,B,C,D].

The numerical discretization is based on radial basis function-generated finite differences (RBF-FD), which provides a geometric flexibility that allows the nodes to follow the time dependent moving boundaries. It must be noted that the RBF-FD is not the only mesh-free discretization method, which means that the methodology presented here could also have been investigated with other mesh-free schemes instead, e.g. the WLS method, although the conclusions may differ from the ones presented in this thesis.

3.1 Radial basis function-generated finite differences

We seek to approximate spatial differential operators by linear combinations,

$$\mathcal{L}f(\boldsymbol{x})|_{\boldsymbol{x}=\boldsymbol{x}_e} \approx \boldsymbol{w} \cdot \boldsymbol{f} = \sum_{i=1}^{n} w_i f_i, \tag{3.1}$$

where $\mathcal{L}$ is a linear spatial operator, $\boldsymbol{w} \in \mathbb{R}^{1\times n}$ contains the RBF-FD weights that approximate $\mathcal{L}f(\boldsymbol{x})$ at evaluation point $\boldsymbol{x} = \boldsymbol{x}_e \in \mathbb{R}^d$ from the function data $\boldsymbol{f} \in \mathbb{R}^n$. To keep things simple, we restrict the focus to the polyharmonic RBF of odd degree $m \in 2\mathbb{N} + 1$,

$$\psi(r) = r^m, \tag{3.2}$$

where $\psi(r) = \psi(\|\boldsymbol{x} - \boldsymbol{x}_i\|_2) \in \mathbb{R}$ is a radial basis function (RBF) centered at $\boldsymbol{x}_i \in \mathbb{R}^d$ in a d-dimensional space. By augmenting RBFs with multivariate

polynomials, $\boldsymbol{p}(\boldsymbol{x}) \in \mathbb{R}^{1\times\ell}$, several advantages can be obtained [43–45, 60–62]. In order to compute the RBF-FD weights, we initially introduce an interpolant as

$$s(\boldsymbol{x}) = \sum_{i=1}^{n} \kappa_i \psi(\|\boldsymbol{x} - \boldsymbol{x}_i\|_2) + \sum_{j=1}^{\ell} \mu_j p_j(\boldsymbol{x}) \tag{3.3}$$

and require the interpolant to match the function data

$$s(\boldsymbol{x}_i) = f_i, \qquad \forall i \in \{1, 2, \ldots, n\}, \tag{3.4}$$

with the additional matching constraints

$$\sum_{i=1}^{n} \kappa_i p_j(\boldsymbol{x}_i) = 0, \qquad \forall j \in \{1, 2, \ldots, \ell\}, \tag{3.5}$$

where $\ell = \binom{P+d}{P}$ is the number of terms in a d-dimensional polynomial of degree P. Enforcing the conditions in (3.4) and (3.5) yields the linear system

$$\begin{bmatrix} \boldsymbol{A} & \boldsymbol{P} \\ \boldsymbol{P}^T & \boldsymbol{O} \end{bmatrix} \begin{bmatrix} \boldsymbol{\kappa} \\ \boldsymbol{\mu} \end{bmatrix} = \begin{bmatrix} \boldsymbol{f} \\ \boldsymbol{0} \end{bmatrix}, \tag{3.6}$$

with $\boldsymbol{A} = A_{ij} = \psi(\|\boldsymbol{x}_i - \boldsymbol{x}_j\|_2) \in \mathbb{R}^{n\times n}$ being the RBF collocation matrix, $\boldsymbol{P} = P_{ij} = \boldsymbol{p}_j(\boldsymbol{x}_i) \in \mathbb{R}^{n\times\ell}$ is the polynomial matrix, while $\boldsymbol{0} \in \mathbb{R}^{\ell}$ and $\boldsymbol{O} \in \mathbb{R}^{\ell\times\ell}$ are zero matrices. Now, applying the linear operator $\mathcal{L}$ to the interpolant and evaluating it a $\boldsymbol{x} = \boldsymbol{x}_e$ gives

$$\mathcal{L}s(\boldsymbol{x})|_{\boldsymbol{x}=\boldsymbol{x}_e} = \sum_{i=1}^{n} \kappa_i \mathcal{L}\psi(\|\boldsymbol{x} - \boldsymbol{x}_i\|_2)|_{\boldsymbol{x}=\boldsymbol{x}_e} + \sum_{j=1}^{\ell} \mu_j \mathcal{L}p_j(\boldsymbol{x})|_{\boldsymbol{x}=\boldsymbol{x}_e}, \tag{3.7}$$

which in matrix-vector notation is expressed as

$$\mathcal{L}s(\boldsymbol{x}) = \begin{bmatrix} \boldsymbol{a} & \boldsymbol{b} \end{bmatrix} \begin{bmatrix} \boldsymbol{\kappa} \\ \boldsymbol{\mu} \end{bmatrix} = \begin{bmatrix} \boldsymbol{a} & \boldsymbol{b} \end{bmatrix} \begin{bmatrix} \boldsymbol{A} & \boldsymbol{P} \\ \boldsymbol{P}^T & \boldsymbol{O} \end{bmatrix}^{-1} \begin{bmatrix} \boldsymbol{f} \\ \boldsymbol{0} \end{bmatrix}, \tag{3.8}$$

where $\boldsymbol{a}$ and $\boldsymbol{b}$ are defined as

$$\boldsymbol{a} = \begin{bmatrix} \mathcal{L}\psi\left(\|\boldsymbol{x} - \boldsymbol{x}_1\|_2\right)|_{\boldsymbol{x}=\boldsymbol{x}_e} \\ \vdots \\ \mathcal{L}\psi\left(\|\boldsymbol{x} - \boldsymbol{x}_n\|_2\right)|_{\boldsymbol{x}=\boldsymbol{x}_e} \end{bmatrix}^T, \quad \boldsymbol{b} = \begin{bmatrix} \mathcal{L}p_1(\boldsymbol{x})|_{\boldsymbol{x}=\boldsymbol{x}_e} \\ \vdots \\ \mathcal{L}p_\ell(\boldsymbol{x})|_{\boldsymbol{x}=\boldsymbol{x}_e} \end{bmatrix}^T. \tag{3.9}$$

Finally, it can be seen from (3.8) that the RBF-FD weights are computed by

$$\begin{bmatrix} \boldsymbol{w} & \boldsymbol{v} \end{bmatrix} = \begin{bmatrix} \boldsymbol{a} & \boldsymbol{b} \end{bmatrix} \begin{bmatrix} \boldsymbol{A} & \boldsymbol{P} \\ \boldsymbol{P}^T & \boldsymbol{O} \end{bmatrix}^{-1} \tag{3.10}$$

which is equivalent to the solution of the linear system

$$\begin{bmatrix} \boldsymbol{A} & \boldsymbol{P} \\ \boldsymbol{P}^T & \boldsymbol{O} \end{bmatrix} \begin{bmatrix} \boldsymbol{w}^T \\ \boldsymbol{v}^T \end{bmatrix} = \begin{bmatrix} \boldsymbol{a}^T \\ \boldsymbol{b}^T \end{bmatrix}. \tag{3.11}$$

After solving for the weights, only $\boldsymbol{w} \in \mathbb{R}^n$ is used to approximate the action of the linear operator $\mathcal{L}$ by the linear combination in equation (3.1). The other weights, $\boldsymbol{v}$, do not contribute to the approximation, see (3.8), as they will only get multiplied by zeros.

Stencil sizes are chosen as a trade-off between accuracy, stability and computational cost. In general, the strategy is to decide on a polynomial degree P, require a stencil size $n \geq \lceil 2\ell \rceil$ and finally determine the polyharmonic RBF degree from

$$m = \begin{cases} P, & \text{if } P \text{ is odd,} \\ P \pm 1, & \text{if } P \text{ is even.} \end{cases} \tag{3.12}$$

In this way, the only choice is on the augmented polynomial degree P, which eventually dictates the convergence rate [43].

Stencils are determined by building and searching a kd-tree with the Euclidean distance as distance measure. An example is illustrated in figure 3.1, where a single RBF-FD stencil is shown for a fifth degree polyharmonic RBF supplemented with fourth degree polynomials and a relative stencil size $n/\ell = 2.5$. Note here that the ghost nodes are included just as if they were regular nodes. However, other studies have shown that advantages may be achieved by using only nodes that lie on the outside of the body tangent [28].

3.2 Node set generation and update strategy

The node set generation and update strategy is inspired by the work in [43, 63], while the algorithm from [64] is used to distribute the nodes. The node generation and update strategy is outlined below, where static and dynamic boundary nodes refer to their variation over time:

1 Generate nodes on the boundary of the computational domain, $\Omega(t)$.

2 Generate background node set with the local node density $\rho_\Omega = \rho_\Omega(\boldsymbol{x})$ that covers $\Omega(t)$ sufficiently.

3 Remove nodes from the background node set if $r_{\text{dyn}} < \rho_\Omega/2$, where r_{stat} is the smallest distance to a static boundary node.

4 Perform node repelling on a subset of each of the static boundary nodes' stencil nodes.

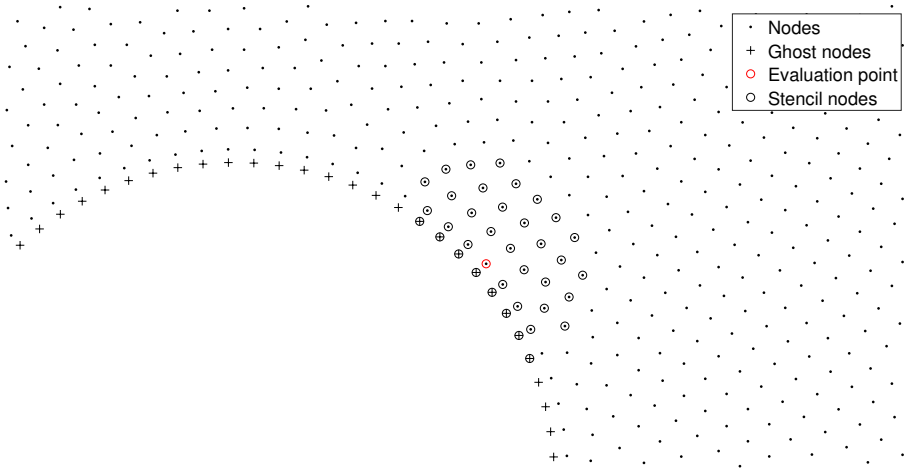

Fig. 3.1: RBF-FD stencil for a fifth degree polyharmonic RBF supplemented with fourth degree polynomials and a relative stencil size $n/\ell = 2.5$.

5 Save the repelled version of the background node set.

6 Remove nodes from the background node set if $r_{\text{dyn}} < \rho_\Omega/2$, where r_{dyn} is the smallest distance to a dynamic boundary node.

7 Perform node repelling on a subset of each of the dynamic boundary nodes' stencil nodes.

8 Remove nodes from the background node set if they are located outside $\Omega(t)$.

9 Repeat step 6-8 at each substep, where the saved background node set from step 5 is re-used each time.

Boundary nodes that are within the subset of a free surface node's stencil are repelled only in the direction tangential to the boundary, which is similar to the strategy in [34].

The node density function $\rho_\Omega = \rho_\Omega(\boldsymbol{x})$ proposed in [A] was a natural extension of the initially proposed formulation in [B], which allows for node refinements near the free surface and moving boundaries. The node density function from [A] is formulated as

$$\rho_\Omega = \begin{cases} \rho_B, & r_{\text{body}} \leq r_{\text{lim}}, \\ \rho_B + (\rho_F - \rho_B)\frac{r_{\text{body}} - r_{\text{lim}}}{r_{\text{bl}} - r_{\text{lim}}}, & r_{\text{lim}} < r_{\text{body}} \leq r_{\text{bl}}, \\ \rho_F, & \text{otherwise}, \end{cases} \tag{3.13}$$

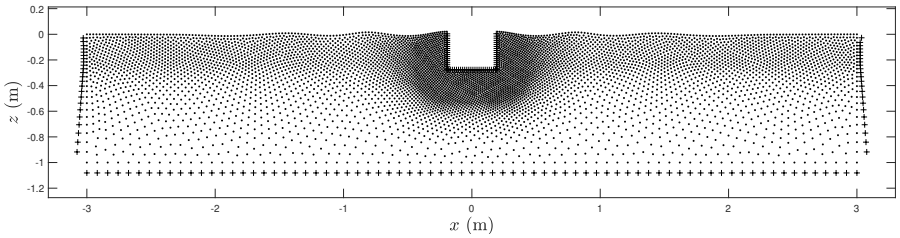

Fig. 3.2: Node set for a heaving rectangular box in a domain with absorption zones near the outer boundaries. Ghost nodes are marked with (+).

where ρ_B is the body node density, r_{body} is the smallest distance to a body boundary node, r_{lim} is the distance at which the node density starts to change and r_{bl} is the distance over which the body node density ρ_B blends together with the fluid node density ρ_F. The fluid node density is the same as the one initially introduced in [B], which is introduced here for the sake of completeness:

$$\rho_F = \rho_{F,\min}(1+\chi), \tag{3.14}$$

where $\rho_{F,\min} = \min(h/N_z)$ is the node density required if the vertical resolution should be equal to N_z nodes at the most shallow region of the domain, $h = h(\boldsymbol{x}_h)$ is the still water depth and $\chi = \chi(\boldsymbol{x})$ is the node distribution function

$$\chi = \begin{cases} \frac{|z|-z_{\text{lim}}}{\min(h)}\rho_{\text{rat}}, & |z| > z_{\text{lim}}, \\ 0, & \text{otherwise}, \end{cases} \tag{3.15}$$

where $z_{\text{lim}} > 0$ specifies an elevation at which the node density begins to change and $\rho_{\text{rat}} = \rho_{F,\max}/\rho_{F,\min}$ is the ratio between maximum and minimum fluid node densities. This allows the node set to be controlled by the parameters N_z, ρ_{rat}, z_{lim}, ρ_B, r_{lim} and r_{bl} and a set of boundary nodes.

Ghost nodes are distributed along the Neumann boundaries with a distance approximately equal to the local node density measure. The ghost nodes are implemented as they improve the diagonal dominance of the Laplace problem, which eases the implementation of an iterative solver. To illustrate the node set generation and update strategy, besides the examples shown in [A,B,C], an example of a node set for a heaving rectangular box in a small domain is illustrated in figure 3.2 with close-ups shown in figure 3.3.

3.3 Time integration

The explicit fourth order Runge-Kutta method is used for evolving the free surface variables in time. In [C], the fully Lagrangian formulations of the free surface variables is used, i.e. $\boldsymbol{t}_w = \nabla\phi/\left\|\nabla\phi\right\|_2$, which require the free surface variables to be re-configured over time by means of interpolation as

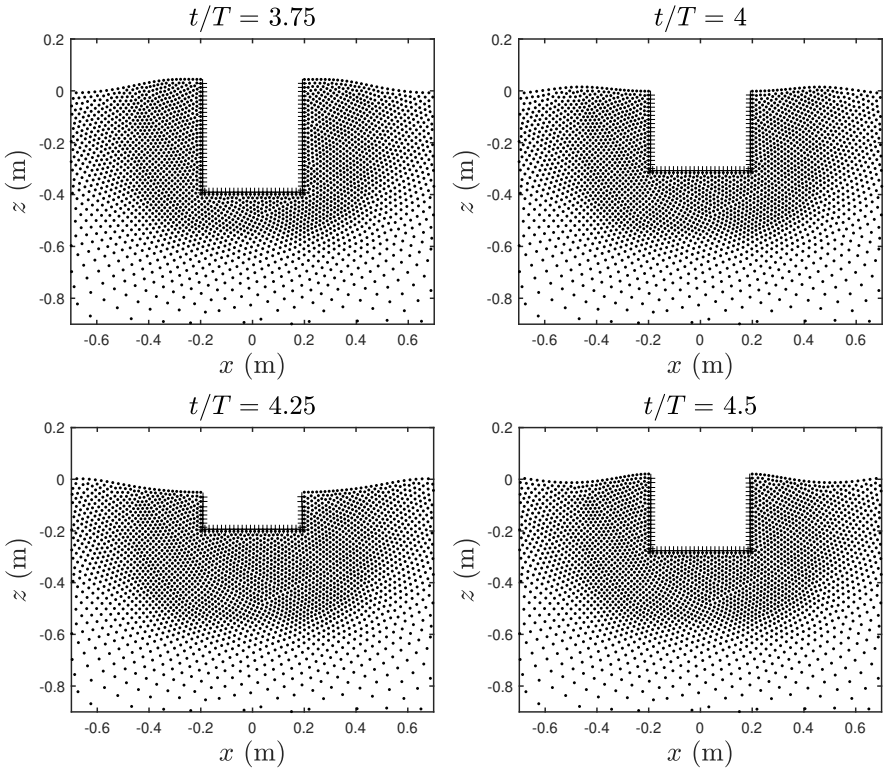

Fig. 3.3: Close-ups of the heaving rectangular box illustrating the node refinements near the moving boundaries. Ghost nodes are marked with (+), although they are difficult to see, they are placed along the submerged part of the moving boundary.

the free surface nodes may get clustered too close together otherwise. The semi-Lagrangian formulations of the free surface conditions are used in [A,B] and the free surface particles are allowed to move in the vertical direction only, i.e. $\boldsymbol{t}_w = \boldsymbol{k}$. This is acceptable because the free surface is considered to be intersected only by lateral boundaries. Other time integration schemes could have been used, but it should be noted that the nature of the Runge-kutta scheme is important if re-configuration of the free surface variables are expected during simulation, as it only requires information of the free surface variables at the current time step. If a multistep scheme is used, the free surface variables have to be interpolated not only at the current time step, but also at previous time steps, in order to be able to step forward in time. Especially, if non-lateral boundaries are intersecting the free surface, it is expected that re-configuration of the free surface variables will be necessary during simulation. However, the direction vector $\boldsymbol{t}_w$ can be used to control the motion of the free surface nodes, which may postpone the need for interpolation of the free surface variables in the vicinity of moving boundaries.

3.4 Hyperviscosity

As described in [C,B], the asymmetric stencils introduce spurious eigenvalues that lead to temporal instabilities. Thus, the system is stabilized by adding a dissipative term to the dynamic and the (vertical) kinematic free surface condition. Let $\gamma = \gamma(\boldsymbol{x}_h)$ denote a hyperviscosity scaling parameter with $\boldsymbol{x}_h \in \mathbb{R}^{d-1}$ being the horizontal position vector, then

$$\frac{D\eta}{Dt} = \mathcal{N}_\eta + \gamma\mathcal{H}\eta, \quad \boldsymbol{x} \in \Gamma_\eta(t), \tag{3.16}$$

$$\frac{D\phi}{Dt} = \mathcal{N}_\phi + \gamma\mathcal{H}\phi, \quad \boldsymbol{x} \in \Gamma_\eta(t), \tag{3.17}$$

where $\mathcal{H} = \Delta_h^k \in \mathbb{R}^{N_\eta \times N_\eta}$ is the kth order Laplace operator in the horizontal dimension(s) with N_η free surface nodes, while $\mathcal{N}_\eta \in \mathbb{R}^{N_\eta}$ and $\mathcal{N}_\phi \in \mathbb{R}^{N_\eta}$ represent the RHSs of the (vertical) kinematic and dynamic free surface conditions in (2.2) and (2.3), respectively.

Scaling of the hyperviscosity operator

A local formulation of the hyperviscosity scaling parameter is proposed in [B] and is expressed as

$$\gamma_i = (-1)^{(k-1)}\gamma_c \left\|\boldsymbol{w}_i\right\|_1^{-1}, \tag{3.18}$$

where γ_c is a control parameter, k is the order of hyperviscosity and $\boldsymbol{w}_i \in \mathbb{R}^{1\times n}$ are the nonzero entries in the ith row vector of the hyperviscosity operator

$\mathcal{H} \in \mathbb{R}^{N_\eta \times N_\eta}$. Knowing that the spectral radius $\rho(\boldsymbol{B})$, for any square matrix $\boldsymbol{B}$, can be bounded from above as

$$\rho(\boldsymbol{B}) = |\lambda|_{max} \leq \|\boldsymbol{B}\|_1 \,, \tag{3.19}$$

with $|\lambda|_{max}$ being the maximum absolute eigenvalue of $\boldsymbol{B}$, the ℓ_1 norm is introduced for the purpose of approximately normalizing the eigenspectrum of the hyperviscosity operator such that the spectral radius $\rho(\gamma\mathcal{H}) \approx \mathcal{O}(\gamma_c)$. Thus, the control parameter γ_c controls the order of the maximum eigenvalue of the scaled hyperviscosity operator and thereby how much the spurious eigenvalues are dissipated. The row wise computations in (3.18) are introduced to differentiate between stencils that are located in regions with different node densities. However, for globally quasi-uniform node sets, it holds that

$$\|\boldsymbol{w}_i\|_1 \approx \|\mathcal{H}\|_1 \,, \qquad \forall i \in \{1, 2, \ldots, N_\eta\} \,, \tag{3.20}$$

which means that the ℓ_1 norm of the hyperviscosity operator can be used for all stencils. Depending on the formulation of the free surface conditions, the hyperviscosity operator may need to be re-computed at every substep. From the investigations in [B], it seems logical to propose a heuristic scaling law based on the formulation in equation (3.18) with a control parameter in the range

$$0.5\omega_N \leq \gamma_c \leq \omega_N, \tag{3.21}$$

where $\omega_N = \sqrt{gk_N \tanh(kh)}$ is the Nyquist frequency as described in [B]. Although the proposed scaling law may provide stable solutions for the discretizations and node sets considered in [A,B,C], it must be stressed that it can not be guaranteed for all discretizations and node sets.

Smoothing near intersection points

It is shown in [A] that the heuristic scaling law in (3.18) may give rise to irregular scaling parameters near boundaries. These irregularities may prevent the hyperviscosity operator from stabilizing the free surface variables sufficiently. Thus, it is illustrated in [A] how the temporal stability may be significantly improved by filtering out the scaling parameter irregularities that may arise near boundaries. Different filtering or smoothing techniques could have been used, but we settle on the moving median filter

$$\gamma_i = \text{median}(\boldsymbol{\gamma}_i), \tag{3.22}$$

where the set of scaling parameters in the stencil of the ith node is

$$\boldsymbol{\gamma}_i = \bigcup_{j=1}^{n} \gamma_{i(j)}, \tag{3.23}$$

where n is the stencil size and $\gamma_{i(j)}$ is the scaling parameter of the jth neighbor in the stencil corresponding to the ith node. The moving median filter is fast to apply and it applies equally well to higher dimensions. The information about stencil neighbors from the RBF-FD weight computations can be utilized again, so no nearest neighbor search is necessary. The moving median filter is applied to all stencils once in [A], but in principle it may be sufficient to apply the filter only to nodes in the vicinity of boundaries that intersect the free surface.

Chapter 4

Scientific contributions

The main scientific contributions of this thesis are mainly constituted by combining the ideas from the studies listed below:

- RBF-FD for geometric flexibility and high-order accuracy [43, 44, 62].
- Mathematical formulations and boundary conditions [16, 25, 57, 59].
- Node distribution and repel algorithms [34, 43, 63, 64].
- Stabilization techniques [40, 65, 66].

The scientific contributions in the papers that compose the main body of this thesis are described in the following.

Paper D & C

The work in [D] illustrates the very first steps of the developments, which included the implementation of RBF-FD for the solution of boundary value problems (BVPs). Based on the work from [D], the model in [C] was developed, which immediately showed that the asymmetric stencils introduced temporal instabilities rapidly. Thus, it was illustrated for the first time that stable two-dimensional and periodic water wave propagation could be achieved by adding hyperviscosity to the free surface variables. This was illustrated to be true for different node sets and augmented polynomial degrees. Additionally, the spatial accuracy was investigated and showed that high-order accuracy could be achieved even without the use of ghost nodes, as expected from the literature [43]. A node generation and update strategy was also developed, which was necessary for discretization the time-dependent fluid domain and to easily tracking the free surface nodes. The fully Lagrangian formulation was used [C] and required the free surface variables to be re-configured after a number of time steps, which was managed by means of interpolation.

Paper B

The findings from [C,D] illustrated that the non-linear potential flow solver based on RBF-FD was possible. However, the main difficulty is to determine a suitable scaling of the hyperviscosity operator, which is the main drawback of using hyperviscosity stabilization, although scaling strategies have been proposed in the literature [65, 66]. By conducting linear stability analyses, it was possible derive a heuristic scaling law based that depends on node density, water depth and RBF-FD discretization [B]. The heuristic scaling law is expected to be suitable for three-dimensional problems as well. It should also be mentioned that the stabilization technique used here may very well be applicable to the work in [47], but also to methods that utilize structured grids, such as [24, 25]. In addition to the stabilization technique, a new node density function was proposed and allowed for node sets to be refined in the vertical direction. This was very useful for the test case in [B], which included variation in the still water depth along the numerical wave tank.

Paper A

In this work, it was noted that the heuristic scaling law from [B] may give rise to instabilities near boundaries, due to irregularities in the scaling parameters. Thus, it was proposed to remove these by a smoothing operation, which should be applicable in both 2- and 3D. For this purpose, a moving median filter was applied to the spatially dependent scaling parameters. This smoothing operation will allow the hyperviscosity operator to stabilize the system to its full extend without introducing new temporal instabilities caused by the scaling parameters. Furthermore, it was in [A] proposed to extend the node density function in [B] to include refinements near the moving boundaries. This was used for significantly decreasing the node set size for a submerged cylinder that experience large amplitude forced motion, which was compared to analytical solutions [A].

Chapter 5

Conclusions

A fully non-linear potential flow model has been developed and implemented in two dimensions. The mathemtical model is based on a mixed-Eulerian-Lagrangian formulation and the spatial discretization is based on radial basis function-generated finite differences, which provides high-order accuracy and geometric flexibility needed for non-linear wave-structure interaction problems. Furthermore, the proposed node generation and update strategy allows to refine the node sets in the vicinity of the free surface and moving boundaries, which makes it possible to use relatively small nodes sets and thus increase the computational efficiency.

A numerical analysis illustrated that the augmented polynomial degree of the RBF-FD dictates the spatial accuracy, which could be expected from the literature. However, the accuracy decreases with increasing wave steepness. An immediate remedy is to use node sets with refinements near the free surface, which will increase the accuracy. It was also found that temporal instabilities may occur rapidly if no stabilization technique is used. The temporal stability is not significantly influenced by the wave steepness, as the instabilities are mainly caused by the asymmetric RBF-FD stencils.

As dissipative terms have been proposed for stabilization purposes previously in the literature, it was natural to test the use of hyperviscosity on the non-linear water wave propagation problem. It was found that stable solutions can be achieved even for wave steepness near the wave breaking limit without significant influence on the model accuracy. Different from previous work is that the dissipative term is added not only to the vertical kinematic free surface condition, but also to the dynamic free surface condition. Similar to previous studies, it was found that applying the Laplace operator repetitively stabilizes the system more efficiently than if the higher-order Laplace operator was computed directly.

As the hyperviscosity operator has to be scaled, it was investigated whether a heuristic scaling law could be derived. This was investigated by conducting linear stability analyses, which illustrated the possibility of scaling the hypervis-

cosity operator by the Nyquist frequency in combination with an approximate ℓ_1 normalization. The heuristic scaling law may require smoothing near boundaries, as irregularities may appear and prevent the hyperviscosity to stabilize the system to its full extent. Different smoothing techniques have been investigated for removing the irregularities. The moving median filter was found to perform well, while it is fast to apply in both two and three dimensions.

The developed model was tested against classical test cases, which include wave propagation over a submerged bar, a standing wave in a bounded domain and the forced motion of a submerged cylinder. These initial test cases illustrate that the stabilized radial basis function-generated finite differences performs well for both non-linear wave propagation problems and wave-structure interaction problems.

5.1 Recommendations for future research

In order to the develop the proposed method further, it is recommended that the following topics are considered:

Complex test cases

It is normal practice to try to break the model that is being developed, in order to understand its weakness. Thus, it is recommended that further test cases are analyzed. Especially, test cases that include free surface intersecting moving boundaries. In that respect, it is natural to consider adaptive node refinements of the free surface nodes in the vicinity of the moving boundaries that intersect the free surface.

Extension to 3D

As the developed model was implemented for two-dimensional problems only, the computational speed was of minor importance. However, for three-dimensional problems the computational cost is bound to become non-trivial. The three most time-consuming tasks are: node updates, RBF-FD weight computation and the linear system of equations related to the Laplace problems. These tasks have to be optimized with respect to computational cost in order to make the model feasible in three dimensions.

Coupling with other models

The developed model may serve as a near-field solver in combination with e.g. the finite difference solver in [24, 25]. Lastly, the coupling with structural models based on the finite element method should also be explored.

References

[1] M. E. Nielsen, M. D. Ulriksen, L. Damkilde, Simulation of Floaters in Action: 1-theory: Release: Sofia v1. 0 (2016).

[2] E. Ransley, S. Yan, S. Brown, M. Hann, D. Graham, C. Windt, P. Schmitt, J. Davidson, J. Ringwood, P.-H. Musiedlak, et al., A blind comparative study of focused wave interactions with floating structures (ccp-wsi blind test series 3) (2020).

[3] C. Fitzgerald, Chapter 5 - nonlinear potential flow models, in: M. Folley (Ed.), Numerical Modelling of Wave Energy Converters, Academic Press, 2016, pp. 83 – 104.

[4] J. Davidson, R. Costello, Efficient nonlinear hydrodynamic models for wave energy converter design—a scoping study, Journal of Marine Science and Engineering 8 (1) (2020) 35.

[5] J. N. Newman, Marine Hydrodynamics, The MIT Press, 1977.

[6] O. M. Faltinsen, Sea loads on ships and offshore structures, Cambridge University Press, 1990.

[7] T. Sarpkaya, Wave forces on offshore structures, Cambridge University Press, 2010.

[8] J. D. Fenton, Numerical methods for nonlinear waves, Advances in Coastal and Ocean Engineering, vol. 5, 1999.

[9] A. Myhr, T. A. Nygaard, Comparison of Experimental Results and Computations for Tension-Leg-Buoy Offshore Wind Turbines, Journal of Ocean and Wind Energy, 2016.

[10] M. E. Nielsen, M. D. Ulriksen, L. Damkilde, SOFIA - A simulation tool for bottom founded and floating offshore structures, Procedia engineering 199 (2017) 1308–1313.

[11] J. Palm, G. Moura Paredes, C. Eskilsson, F. Taveira Pinto, L. Bergdahl, Simulation of mooring cable dynamics using a discontinuous galerkin

method, in: 5th International Conference on Computational Methods in Marine Engineering, MARINE 2013; Hamburg; Germany; 29 May 2013 through 31 May 2013, 2013, pp. 455–466.

[12] M. Hall, A. Goupee, Validation of a lumped-mass mooring line model with deepcwind semisubmersible model test data, Ocean Engineering 104 (2015) 590 – 603.

[13] C.-H. Lee, WAMIT theory manual, MIT, 1995.

[14] A. Babarit, G. Delhommeau, Theoretical and numerical aspects of the open source BEM solver NEMOH, In Proc. of the 11th European Wave and Tidal Energy Conference, 2016.

[15] W. E. Cummins, The impulse response function and ship motions, Schiffstechnik, 1962.

[16] Y. Liu, M. Xue, D. K. Yue, Computations of fully nonlinear three-dimensional wave–wave and wave–body interactions. part 2. nonlinear waves and forces on a body, Journal of Fluid Mechanics 438 (2001) 41–66.

[17] E. Guerber, M. Benoit, S. T. Grilli, C. Buvat, A fully nonlinear implicit model for wave interactions with submerged structures in forced or free motion, Engineering Analysis with Boundary Elements 36 (7) (2012) 1151–1163.

[18] E. Dombre, M. Benoit, D. Violeau, C. Peyrard, S. Grilli, Simulation of floating structure dynamics in waves by implicit coupling of a fully nonlinear potential flow model and a rigid body motion approach, Journal of Ocean Engineering and Marine Energy 1 (1) (2015) 55–76.

[19] K. Tanizawa, A nonlinear simulation method of 3-d body motions in waves (1st report), Journal of the Society of Naval Architects of Japan 1995 (178) (1995) 179–191.

[20] K. Tanizawa, A nonlinear simulation method of 3-d body motions in waves: Formulation with the acceleration potential, in: 10th International Workshop on Water Waves and Floating Bodies, 1995.

[21] M. Xue, H. Xü, Y. Liu, D. K. Yue, Computations of fully nonlinear three-dimensional wave–wave and wave–body interactions. part 1. dynamics of steep three-dimensional waves, Journal of Fluid Mechanics 438 (2001) 11–39.

[22] S. T. Grilli, P. Guyenne, F. Dias, A fully non-linear model for three-dimensional overturning waves over an arbitrary bottom, International Journal for Numerical Methods in Fluids 35 (7) (2001) 829–867.

[23] B. Li, C. A. Fleming, A three dimensional multigrid model for fully nonlinear water waves, Coastal Engineering 30 (3-4) (1997) 235–258.

[24] H. B. Bingham, H. Zhang, On the accuracy of finite-difference solutions for nonlinear water waves, Journal of Engineering Mathematics 58 (1-4) (2007) 211–228.

[25] A. P. Engsig-Karup, H. B. Bingham, O. Lindberg, An efficient flexible-order model for 3D nonlinear water waves, Journal of Computational Physics 228 (6) (2009) 2100–2118.

[26] O. Lindberg, H. B. Bingham, A. P. Engsig-Karup, Towards real time simulation of ship-ship interaction-part iii: Immersed body boundary condition and double body ship-ship interaction, in: 29th International Workshop on Water Waves and Floating Bodies, 2014.

[27] S. Kontos, H. B. Bingham, O. Lindberg, A. P. Engsig-Karup, On nonlinear wave-structure interaction using an immersed boundary method in 2d, in: 31th International Workshop on Water Waves and Floating Bodies (IWWWFB 2016), 2016.

[28] S. Kontos, Robust numerical methods for nonlinear wave-structure interaction in a moving frame of reference, Technical University of Denmark, 2016.

[29] J. Hicks, H. B. Bingham, O. Lindberg, A. P. Engsig-Karup, Incorporating a semi-lagrangian body-free-surface intersection point in a fully nonlinear potential model, in: 35th International Workshop on Water Waves and Floating Bodies (IWWWFB 2020), 2020.

[30] Y. Xu, H. B. Bingham, Y. Shao, Finite difference solutions for nonlinear water waves using an immersed boundary method, in: 35th International Workshop on Water Waves and Floating Bodies (IWWWFB 2020), 2020.

[31] S. Ma, F.-C. Hanssen, M. A. Siddiqui, M. Greco, O. M. Faltinsen, Local and global properties of the harmonic polynomial cell method: In-depth analysis in two dimensions, International Journal for Numerical Methods in Engineering 113 (4) (2018) 681–718.

[32] F.-C. W. Hanssen, Non-linear wave-body interaction in severe waves (2019).

[33] F.-C. Hanssen, A. Bardazzi, C. Lugni, M. Greco, Free-surface tracking in 2d with the harmonic polynomial cell method: Two alternative strategies, International Journal for Numerical Methods in Engineering 113 (2) (2018) 311–351.

[34] S. Yan, Q. Ma, Numerical simulation of fully nonlinear interaction between steep waves and 2d floating bodies using the qale-fem method, Journal of Computational physics 221 (2) (2007) 666–692.

[35] Q. W. Ma, S. Yan, Qale-fem for numerical modelling of non-linear interaction between 3d moored floating bodies and steep waves, International Journal for Numerical Methods in Engineering 78 (6) (2009) 713–756.

[36] Q. Ma, S. Yan, Quasi ale finite element method for nonlinear water waves, Journal of computational physics 212 (1) (2006) 52–72.

[37] G. Wu, R. E. Taylor, Finite element analysis of two-dimensional non-linear transient water waves, Applied Ocean Research 16 (6) (1994) 363–372.

[38] G. Wu, Q. Ma, R. E. Taylor, Numerical simulation of sloshing waves in a 3d tank based on a finite element method, Applied ocean research 20 (6) (1998) 337–355.

[39] S. Yan, Q. Ma, Qale-fem for modelling 3D overturning waves, International Journal for Numerical Methods in Fluids 63 (6) (2010) 743–768.

[40] I. Robertson, S. Sherwin, Free-surface flow simulation using hp/spectral elements, Journal of Computational Physics 155 (1) (1999) 26–53.

[41] C. M. Sanchez, A. P. Engsig-Karup, C. Eskilsson, Nonlinear wave-body interaction using a mixed-eulerian-lagrangian spectral element model, in: 37th International Conference on Ocean, Offshore and Artic Engineering (OMAE2018), 2018.

[42] A. P. Engsig-Karup, C. Monteserin, C. Eskilsson, A mixed eulerian–lagrangian spectral element method for nonlinear wave interaction with fixed structures, Water Waves 1 (2) (2019) 315–342.

[43] V. Bayona, N. Flyer, B. Fornberg, G. A. Barnett, On the role of polynomials in RBF-FD approximations: II. Numerical solution of elliptic PDEs, Journal of Computational Physics 332 (2017) 257–273.

[44] N. Flyer, G. A. Barnett, L. J. Wicker, Enhancing finite differences with Radial Basis Functions: Experiments on the Navier–Stokes equations, Journal of Computational Physics 316 (2016) 39–62.

[45] B. Fornberg, N. Flyer, Solving PDEs with Radial Basis Functions, Acta Numerica 24 (2015) 215–258.

[46] U. Senturk, Modeling nonlinear waves in a numerical wave tank with localized meshless rbf method, Computers & Fluids 44 (1) (2011) 221–228.

[47] C. Raoult, M. Benoit, M. L. Yates, Development and validation of a 3d rbf-spectral model for coastal wave simulation, Journal of Computational Physics 378 (2019) 278–302.

[48] J. Palm, C. Eskilsson, G. M. Paredes, L. Bergdahl, Coupled mooring analysis for floating wave energy converters using cfd: Formulation and validation, International Journal of Marine Energy 16 (2016) 83 – 99.

[49] O. Lindberg, Multiscale Simulation of Breaking Wave Impacts, Technical University of Denmark, 2013.

[50] A. Crespo, J. Domínguez, B. Rogers, M. Gómez-Gesteira, S. Longshaw, R. Canelas, R. Vacondio, A. Barreiro, O. García-Feal, Dualsphysics: Open-source parallel cfd solver based on smoothed particle hydrodynamics (sph), Computer Physics Communications 187 (2015) 204 – 216.

[51] B. Ren, M. He, P. Dong, H. Wen, Nonlinear simulations of wave-induced motions of a freely floating body using wcsph method, Applied Ocean Research 50 (2015) 1 – 12.

[52] C. Eskilsson, J. Palm, J. P. Kofoed, E. Friis-Madsen, Cfd study of the overtopping discharge of the wave dragon wave energy converter, Renewable Energies Offshore (2015) 287–294.

[53] T. Verbrugghe, J. M. Domínguez, A. J. Crespo, C. Altomare, V. Stratigaki, P. Troch, A. Kortenhaus, Coupling methodology for smoothed particle hydrodynamics modelling of non-linear wave-structure interactions, Coastal Engineering 138 (2018) 184–198.

[54] T. Kristiansen, O. M. Faltinsen, Gap resonance analyzed by a new domain-decomposition method combining potential and viscous flow draft, Applied Ocean Research 34 (2012) 198 – 208.

[55] S. Yan, J. Wang, J. Wang, Q. Ma, Z. Xie, et al., Numerical simulation of wave structure interaction using qalefoam, in: The 29th International Ocean and Polar Engineering Conference, International Society of Offshore and Polar Engineers, 2019.

[56] N. Zhang, S. Yan, X. Zheng, Q. Ma, et al., A 3d hybrid model coupling sph and qale-fem for simulating nonlinear wave-structure interaction, International Journal of Offshore and Polar Engineering 30 (01) (2020) 11–19.

[57] A. P. Engsig-Karup, S. L. Glimberg, A. S. Nielsen, O. Lindberg, Fast hydrodynamics on heterogeneous many-core hardware, Designing Scientific Applications on GPUs (2013) 251–294.

[58] J. Larsen, H. Dancy, Open boundaries in short wave simulations—a new approach, Coastal Engineering 7 (3) (1983) 285–297.

[59] N. G. Jacobsen, D. R. Fuhrman, J. Fredsøe, A wave generation toolbox for the open-source cfd library: Openfoam®, International Journal for numerical methods in fluids 70 (9) (2012) 1073–1088.

[60] V. Bayona, N. Flyer, B. Fornberg, On the role of polynomials in rbf-fd approximations: Iii. behavior near domain boundaries, Journal of Computational Physics 380 (2019) 378–399.

[61] V. Bayona, An insight into rbf-fd approximations augmented with polynomials, Computers & Mathematics with Applications 77 (9) (2019) 2337–2353.

[62] V. Bayona, Comparison of moving least squares and rbf+ poly for interpolation and derivative approximation, Journal of Scientific Computing 81 (1) (2019) 486–512.

[63] B. Fornberg, N. Flyer, Fast generation of 2-D node distributions for mesh-free PDE discretizations, Computers and Mathematics with Applications 7 (69) (2015) 531–544.

[64] K. van der Sande, B. Fornberg, Fast variable density 3-d node generation, arXiv preprint arXiv:1906.00636 (2019).

[65] B. Fornberg, E. Lehto, Stabilization of RBF-generated finite difference methods for convective PDEs, Journal of Computational Physics 230 (6) (2011) 2270–2285.

[66] V. Shankar, A. L. Fogelson, Hyperviscosity-based stabilization for radial basis function-finite difference (RBF-FD) discretizations of advection–diffusion equations, Journal of Computational Physics 372 (2018) 616–639.

Part II

Papers

ISSN (online): 2446-1636
ISBN (online): 978-87-7210-802-5 AALBORG UNIVERSITY PRESS